ISSN1027-5495. Functional Materials, 32, No.1 (2025), p. 77-86
doi:http://dx.doi.org/10.15407/fm32.01.77 © 2025 — STC "Institute for Single Crystals"

Microstructure, dynamics, and temperature behavior of *L*-menthol, salicylaldoxime, and their binary mixture: a molecular dynamics simulation study

M. Yu. Cherniakova,[1] A.V. Kyrychenko,[1,2] K. N. Belikov[1,3]*

[1] Institute of Functional Materials Chemistry, State Scientific Institution "Institute for Single Crystals", National Academy of Sciences of Ukraine, 60 Nauky Ave., Kharkiv 61072, Ukraine
[2] Institute of Chemistry and School of Chemistry, V. N. Karazin Kharkiv National University, 4 Svobody Sq., Kharkiv 61022, Ukraine.
[3] School of Chemistry, V. N. Karazin Kharkiv National University, 4 Svobody Sq., Kharkiv 61022, Ukraine.

Received January 10, 2025

Deep eutectic solvents are mixtures of various substances classified as liquid supramolecular systems, which have a wide range of scientific, practical, and technological applications. This study investigated the molecular aspects involved in creating a deep eutectic binary mixture of *L*-menthol and salicylaldoxime using classical molecular dynamics simulations. We focused on the microstructure and dynamics of intermolecular interactions for both the individual components and their binary mixture at temperatures of 298, 333, and 353 K. Our findings revealed that, at a macroscopic scale, there is a nearly uniform distribution of components in the binary mixture of *L*-menthol and salicylaldoxime, with no phase separation or domain formation observed within the examined temperature range. We noted a significant increase in self-diffusion coefficients in the formation of the binary mixture, with these coefficients further increasing at higher temperatures. Through hydrogen bonding analysis and radial distribution functions, we demonstrated that the formation of the binary mixture resulted in changes to the solution's microstructure, including a considerable reduction in the number of intermolecular hydrogen bonds. Consequently, the transition to a liquid phase at room temperature for this eutectic composition is primarily driven by van-der-Waals attractions between the hydrophobic portions of the components. Our theoretical findings are significant from both scientific and practical perspectives, as they provide valuable insights into the relationship between the microscopic structure of a deep eutectic mixture and its transport properties.

Keywords: deep eutectic solvent, binary mixture, solution microstructure, intermolecular interaction, molecular dynamics modeling, supramolecular chemistry, organized molecular system.

Мікроструктура, динаміка та температурна поведінка *L*-ментолу, саліцилальдоксиму та їх бінарної суміші: молекулярно-динамічне дослідження. *М.Ю. Чернякова, О.В. Кириченко, К.М. Беліков*.

Глибокоевтектичні розчинники - це суміші різних речовин, що класифікуються як рідкі супрамолекулярні системи, які мають широкий спектр наукових, практичних і технологічних застосувань. У цьому дослідженні ми вивчали молекулярні аспекти створення глибокоевтектичної бінарної суміші *L*-ментолу та саліцилальдоксиму, використовуючи класичне молекулярно-динамічне моделювання. Мікроструктуру та динаміку міжмолекулярних взаємодій було досліджено як для окремих компонентів, так і для їх бінарної суміші при

температурах 298, 333 і 353 К. Наші результати показали, що на макроскопічному рівні спостерігається майже рівномірний розподіл компонентів у бінарній суміші *L*-ментолу і саліцилальдоксиму, без фазового поділу або утворення доменів у досліджуваному температурному діапазоні. Значне збільшення коефіцієнтів самодифузії спостерігалося при утворенні бінарної суміші, причому ці коефіцієнти ще більше зростали при більш високих температурах. За допомогою аналізу водневих зв'язків і функцій радіального розподілу ми продемонстрували, що утворення бінарної суміші призводить до зміни мікроструктури розчину, в тому числі до значного зменшення кількості міжмолекулярних водневих зв'язків. Отже, перехід у рідку фазу при кімнатній температурі для цієї евтектичної композиції зумовлений насамперед взаємодією Ван-дер-Ваальса між гідрофобними частинами компонентів. Наші теоретичні висновки є важливими як з наукової, так і з практичної точки зору, оскільки вони дають цінне уявлення про взаємозв'язок між мікроскопічною структурою глибокоевтектичної суміші та її транспортними властивостями.

1. Introduction

Deep eutectic solvents (DES) have garnered significant interest from the scientific community for their potential technological applications in sustainable chemistry. DES are mixtures of different substances and can be considered as liquid supramolecular systems. A key characteristic of DES is their notably depressed melting temperature, which arises from strong intermolecular interactions, particularly a network of hydrogen bonds (H-bonds) between the components of the mixture [1]. These components include H-bond acceptors (HBA) and H-bond donors (HBD). However, only a limited number of combinations of HBA and HBD can demonstrate this property, which is why the broader term "eutectic solvents" (ES) is recommended for general use [2].

The tunability of ES allows them to be utilized as customized environmentally friendly solvents with specific properties tailored for particular applications, such as separation technologies and extraction processes [2-4]. Hydrophobic ES show great promise in extracting both organic and inorganic compounds from aqueous media due to their high extraction efficiency and ability to recover solvents [5-6]. Hydrophobic ES are composed of low water-soluble substances, often combinations of various compounds, including:

- Terpene compounds (such as thymol and menthol) [7],
- Long-chain carboxylic acids (like octanoic and decanoic acids) [8],
- Hydroxy- and polycarboxylic acids (for example, salicylic and phthalic acids) [9-10],
- Long-chain alcohols (such as octanol and tetradecanol) [11-12],
- Tetraalkyl organic salts (including methyltrioctylammonium chloride and 1-decyl-3-methylimidazolium chloride) [13-14],
- Other compounds (such as phenol, salol, vanillin, and 8-hydroxyquinoline) [15-17].

Research on the extraction performance of these environmentally friendly solvents and their application as extraction systems primarily focuses on organic and inorganic pollutants, toxicants, compounds derived from plants and animals, and pharmaceuticals [2, 18-19].

Recently, a new DES comprising a chelating agent for metal ions was introduced [20]. This DES is a mixture of menthol and salicylaldoxime, with a melting temperature of approximately -52 °C, depending on the specific molar ratios of its components. Although there is some available data on the physicochemical properties of this system, it is insufficient for a complete understanding of the molecular interactions between the components. In this context, conducting a study using molecular dynamics (MD) simulation offers significant advantages for characterizing the DES.

The solid-liquid phase behavior of the menthol: salicylaldoxime system [20] is similar to that observed in a mixture of menthol and thymol [7]. MD studies have demonstrated that small hydrogen-bonded clusters form in the liquid phase of the menthol:thymol mixture [21]. The number of H-bonds per thymol molecule was found to be 0.46 and 0.61 for 1:1 and 2:1 ratios of the components, respectively [22]. The self-diffusion coefficients for menthol and thymol were measured at 1.33×10^{-11} and 1.66×10^{-11} m²/s in the 1:1 mixture, while in the 2:1 mixture, they were 0.85×10^{-11} and 1.05×10^{-11} m²/s, respectively [23]. H-bonding was also confirmed in mixtures of menthol with hexanoic, octanoic, decanoic, and lauric acids. However, this bonding was observed on a short time scale, and the frequency of interactions between the components decreased as the hydrocarbon chain length of the acid increased [24-25].

Atomistic MD simulations have emerged as a powerful computational tool that complements experimental studies of thermodynamic and

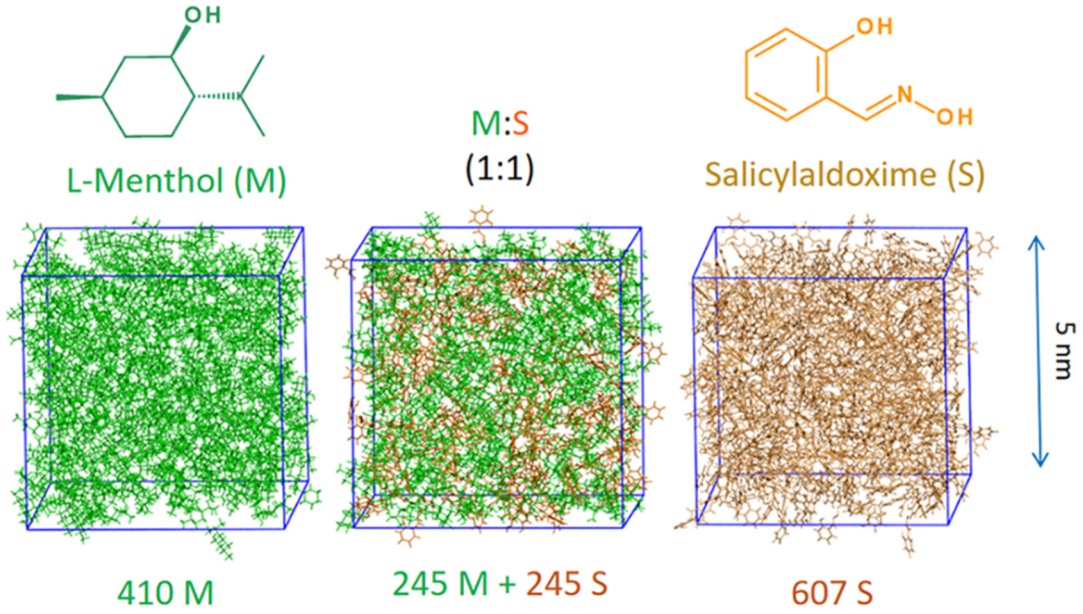

Fig. 1. Molecular structures of **M** and S (*top*). Examples of MD snapshots of the **M**, S and their 1:1 binary mixture in equilibrium (bottom).

transport processes in DES at the atomic level [23, 26-27]. These simulations provide valuable insights into the fundamental phenomena of these systems [28]. In this work, we utilize all-atom MD simulations to conduct a detailed exploration of the structure and dynamic behavior of the M:S mixture, particularly focusing on its temperature-dependent characteristics at the microscopic level.

2. Computational details

MD Simulations. All-atom OPLS force field (FF) parameters were used for *L*-menthol and salicylaldoxime [29]. Molecular topologies were generated using LigParGen web-tool [30]. All MD simulations were performed for the NPT ensemble. The reference temperature of 298.15, 333, and 353 K was maintained constant using the v-rescale weak coupling scheme [31] with a constant τ_T=0.1 ps. A constant pressure of 1 atm was maintained using a Parrinello-Rahman barostat with a constant τ_P=1 ps. The initial atomic velocities were generated with a Maxwell distribution at a given absolute temperature. Periodic boundary conditions were applied to all three directions of the modeled box. The electrostatic interactions were modeled using the Ewald approach (PME) [32] with a long-range cutoff of 1.1 nm. The boundary distance of the Lennard-Jones interaction was also 1.1 nm. The MD simulation step was 2 fs with the neighbor list updated every 10 fs. All bond lengths were kept constant using the LINCS subroutine [33-34]. MD simulations were performed using the GROMACS software package, version 2019.4 [35]. Molecular graphics and visualization were performed using VMD 1.9.3 [36] and BIOVIA Discovery Studio Visualizer.

3. Results and discussion

System setup. A cubic box measuring approximately 50 Å on each side was filled with *L*-menthol (**M**) or salicylaldoxime (**S**) molecules by randomizing their initial atomic positions. This process allowed us to incorporate 410 **M** molecules and 607 **S** molecules, as shown in Figure 1. Additionally, the same-sized box was filled with a randomly distributed mixture of **M** and **S**, which could accommodate up to 245 molecules of each component.

For each system, the MD simulation process consists of four main steps:

1. Energy minimization is conducted to eliminate any close contacts between molecules.

2. A 5-ns canonical simulation (NVT) is performed at a temperature of 353 K, which is above the experimentally determined melting points for all components.

3. A 5-ns isobaric-isothermal simulation (NPT) is then carried out at 1 atm pressure, allowing the system to reach thermodynamic equilibrium at the specified temperatures of 298, 333, or 353 K, respectively.

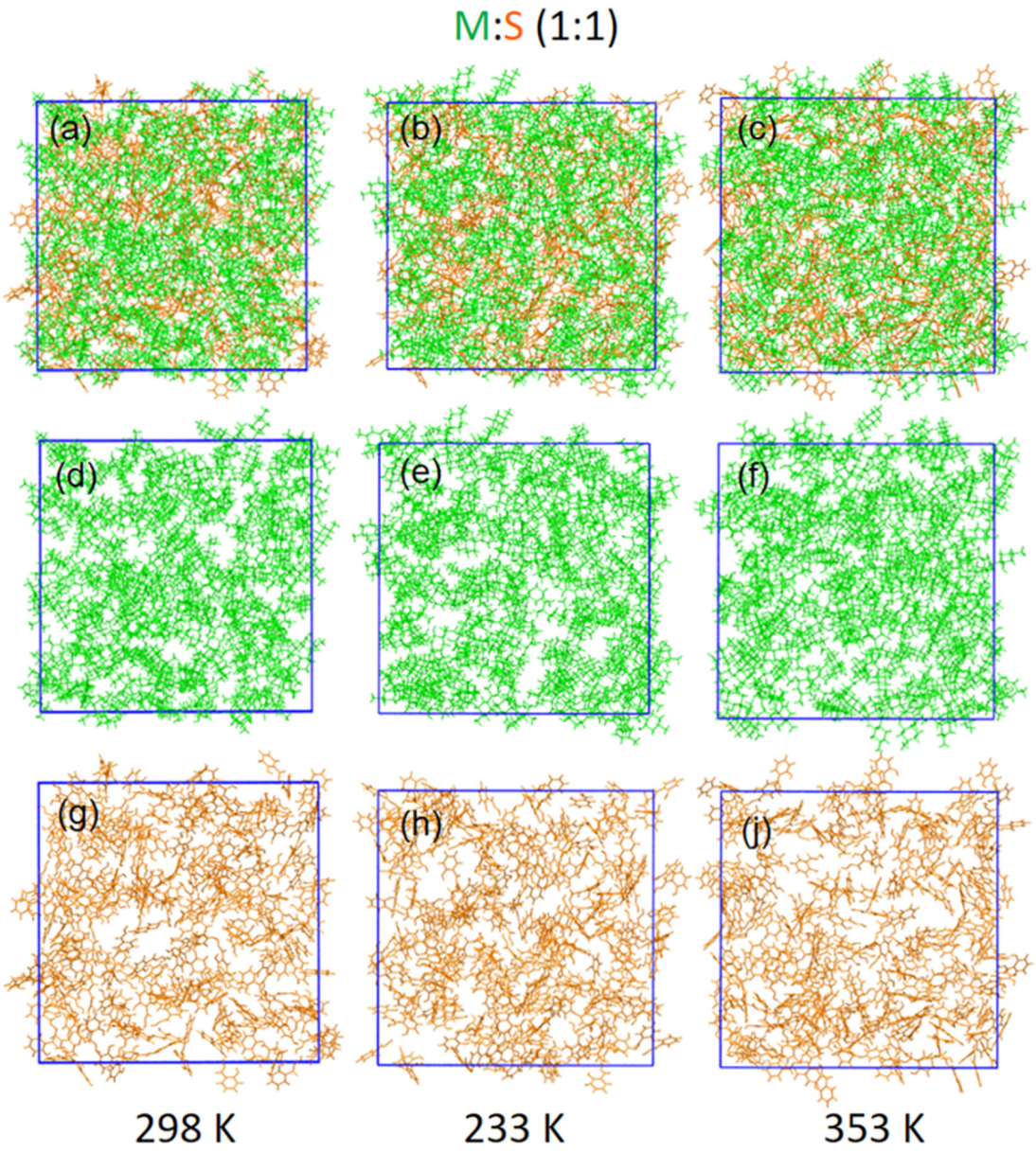

Fig. 2. MD snapshots of the equilibrated configuration for **M**:**S** mixture containing 245 **M** and 245 **S** molecules taken at three different temperatures: 298 K (a), 333 K (b) and 353 K (c). Panels *d-j* illustrate distribution of individual components in these binary mixtures: 245 **M** (*d-f*) and 245 **S** (*g-j*) molecules, respectively.

4. Finally, a 200-ns productive MD simulation is executed to collect data at intervals of 20 ps.

The atomistic description of the structural arrangement among the different components is performed for the pure components **M** and **S**, as well as their 1:1 mixture (see Fig. 1).

Microstructure of M:S (1:1) Mixture. Some hydrophobic DES have been found to exhibit structural and dynamic microheterogeneity [24, 37]. This microheterogeneity arises from the non-uniform distribution of components at the molecular level, which is influenced by H-bonding and the separation of polar and non-polar regions [28, 37-38]. This phenomenon has been thoroughly investigated for other menthol-containing DES using experimental techniques, such as small-angle X-ray scattering (SAXS), FTIR, NMR, and MD simulations [24, 37, 39-40].

Figure 2 illustrates that, at a macroscopic level, the components **M** and **S** are nearly uniformly distributed in the binary **M**:**S** mixture, regardless of the temperature studied. Additionally, the binary **M**:**S** system shows no signs

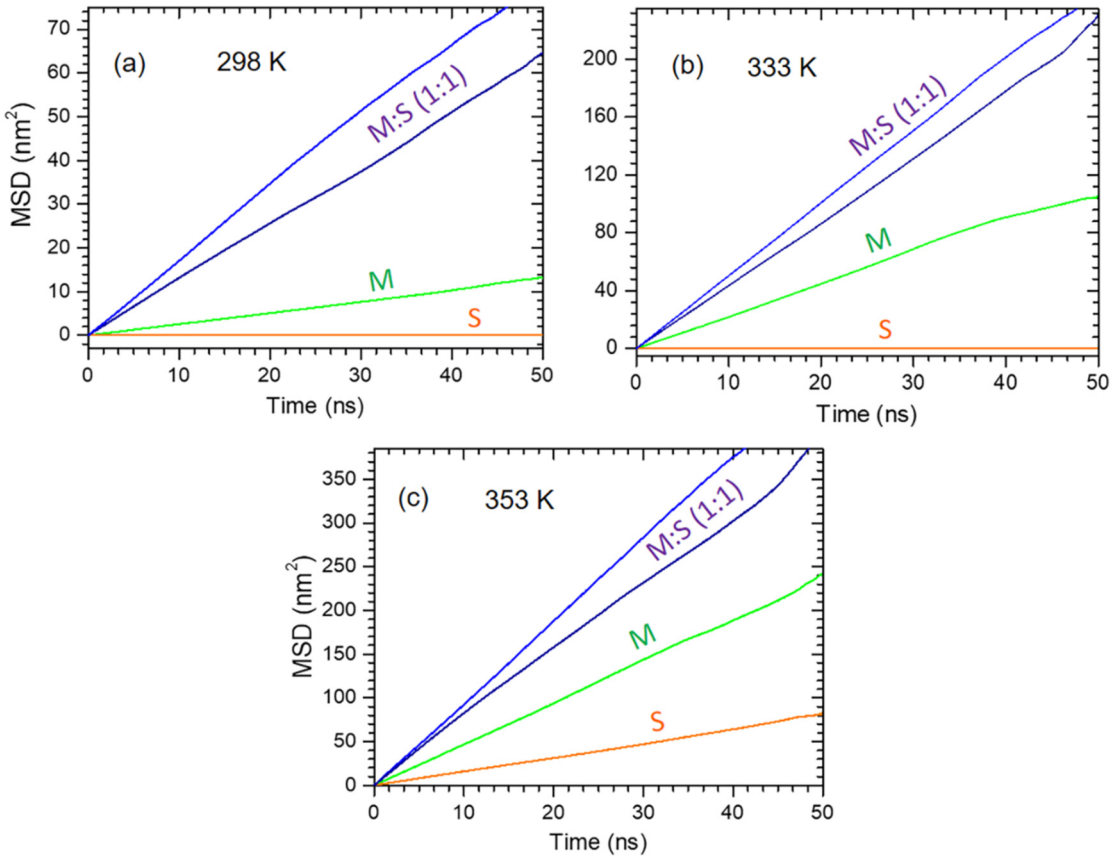

Fig. 3. MSDs in pure **M**, **S** and their 1:1 mixture at different temperatures 298 K (*a*), 333 K (*b*) and 353 K (*c*), respectively. For the binary mixture, MSD is shown for each competent separately.

of phase separation or domain formation within the examined temperature range.

Self-diffusion coefficients. Self-diffusion coefficients (D_s) are a critical property of DES as they provide insights into the molecular mobility and dynamics within the solvent [22]. They quantify how quickly molecules move within the solution due to random thermal motion [24].

Coefficients D_s of pure **M** and **S** components and their mixture were calculated from the mean square displacement (MSD) using Eq. 1:

$$D_s = \frac{1}{6}\lim_{t\to\infty}\frac{d\left|r_j(t)-r_j(0)\right|^2}{dt}, \qquad (1)$$

where $r_j(t)-r_j(0)$ is a measure of molecule displacement between time 0 and time t.

Coefficients D_s were then calculated from the slope of the corresponding MSDs in Fig. 3 using the Einstein relation and summarized in Table 1.

From Table 1, it can be noted that the coefficients D_s for the individual components of the **M**:**S** mixture increase essentially compared to those in the pure **M** and **S**. This trend was observed for all three studied temperatures. Qualitatively, this effect can be attributed to the dramatic decrease in the viscosity of the mixture due to formation of eutectic state.

Intermolecular H-Bonding Interactions. Numerous evidences have demonstrated that H-bonding between two or more components plays an essential role in the formation of an eutectic mixture [5, 28, 41]. MD simulations have been used to study the structure and dynamics of the formation and breaking of H-bonds in DES [24].

To analyze intermolecular H-bonding, we employed specific geometric cut-off criteria for H-bond formation. A H-bond was considered to occur when two geometric conditions (distance and angle) were met: (*1*) The distance r_i between the Hydrogen and Oxygen atoms must be $r_i \le r_{HB}$ =2.5 Å (this cutoff value corresponds to the first minimum of radial distribution functions of the simple point-charge model (SPC) of water); (2) the angle O···H–O should satisfy $\alpha_i \le \alpha_{HB}$=0±30°. These geometric criteria are commonly used in analyzing H-bonded complexes [42-43]. The total number of hydrogen bonds was calculat-

Table 1. Coefficients D_s of pure **M**, **S** and their 1:1 mixture simulated at three different temperatures. For the binary mixture, the coefficients are shown for each component separately.

Temperature	System	Component	Self-diffusion coefficient, D_s ($\times 10^{-5}$ cm^2/s)
298 K	pure M		0.043
	pure S		0.0001
	M:S (1:1)	M	0.21
		S	0.27
333 K	pure M		0.38
	pure S		0.0014
	M:S (1:1)	M	0.75
		S	0.84
353 K	pure M		0.74
	pure S		0.26
	M:S (1:1)	M	1.23
		S	1.57

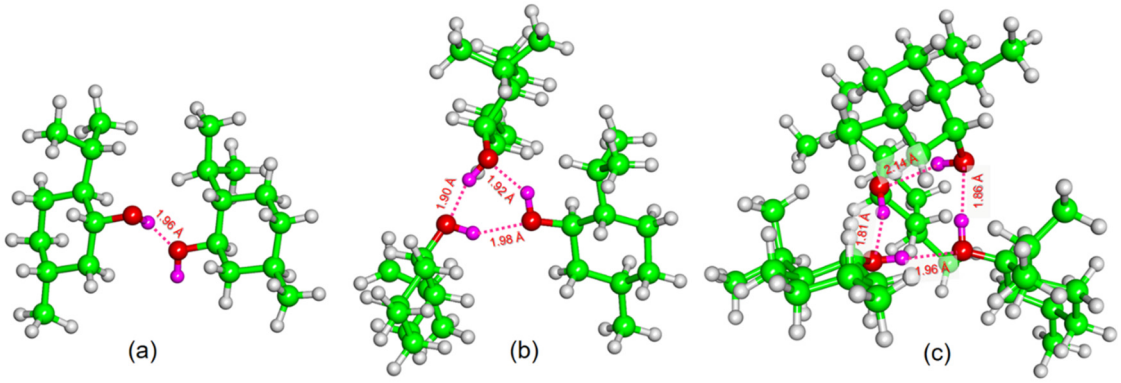

Fig. 4. Representative MD snapshots of some typical H-bonded structures observed in bulk **M** at 298.15 K: H-bonded dimer (*a*), cyclically H-bonded trimer (*b*) and tetramer (*b*), respectively. The red dashed lines represent H-bonding interactions and their corresponding distances between hydroxyl groups.

ed for each 100 ps time frame during the last 10 ns of the MD sampling.

The analysis of H-bonding interactions in pure bulk **M** revealed that **M** molecules do not form a permanent long-range H-bonded network. Instead, some intermediate-range structural heterogeneity was observed, as evidenced by the formation of some local H-bonded aggregates of the different stoichiometry. Figure 4 illustrates some stable H-bonded structures observed in bulk **M** at 298 K. As reported earlier, **M** molecules can form H-bonded dimers and trimers, as seen in Fig. 4*a*-*b*. However, the most **M** molecules tend to form cyclic, H-bonded tetramers (Fig. 4*c*).

The total number of H-bonds in bulk **M** was found to be 290±9, 219±10 and 181±10 at 298, 333 and 353 K, respectively. So, the increase in temperature led to the decrease in the average number of H-bonds per one **M** molecule from 0.71±0.02 up to 0.44±0.02, as summarized in Table 2.

In contrast to bulk **M**, H-bonding in bulk **S** differs significantly. While some stable H-bonded dimers and trimers can also be identified (see Fig. 5*a*-*b*), the majority of the molecular population forms an extensive three-dimensional network of H-bonds. This network can extend along up to ten molecules, as illustrated in Fig. 5*c*. As the temperature rises from 298 to 353 K, some H-bonds break, causing the average number of H-bonds per **S** molecule to decrease from 1.84±0.02 to 1.66±0.04, as shown in Table 2.

Overall H-bonding in the binary mixture of **M** and **S** was surprisingly reduced (Table 2). While some H-bonding between **M** molecules (**M-M**) was still observed, interactions among **S-S** molecules were almost completely diminished. Both **M** and **S** molecules can act as either H-bond donors or acceptors. However, in most cases, only two types of H-bonded heterodimers were observed, in which **M** molecules were

Table 2. H-bonding characteristics for pure **M**, **S** and their components simulated at three different temperatures. For the binary mixture, the coefficients are shown for each component separately.

Temperature	System	Pairwise interaction of components	Total number of H-bonds	Number of H-bonds per molecule
298 K	M	M-M	290±9	0.71±0.02
	S	S-S	1119±12	1.84±0.02
	M:S (1:1)	M-M	87±7	0.39±0.03
		M-S	54±7	0.12±0.03
		S-S	4±2	0.02±0.01
333 K	M	M-M	219±10	0.53±0.02
	S	S-S	1084±15	1.79±0.03
	M:S (1:1)	M-M	65±6	0.29±0.03
		M-S	46±7	0.10±0.03
		S-S	4±2	0.02±0.01
353 K	M	M-M	181±10	0.44±0.02
	S	S-S	1009±22	1.66±0.04
	M:S (1:1)	M-M	50±6	0.22±0.03
		M-S	40±6	0.09±0.03
		S-S	3±2	0.01±0.01

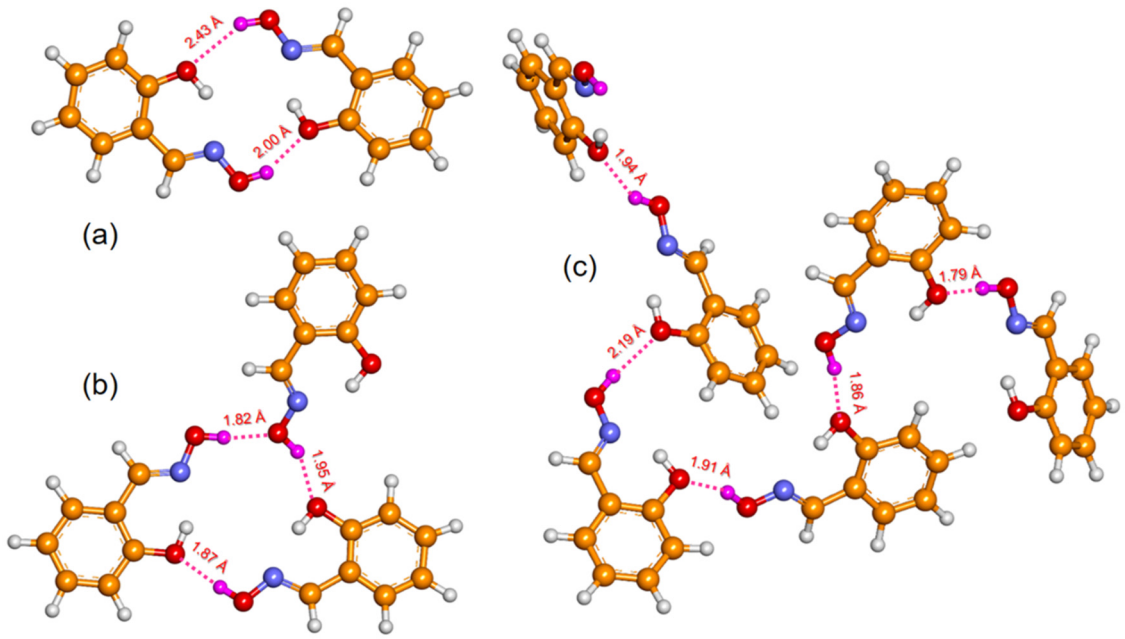

Fig. 5. Representative MD snapshots of H-bonded dimer (*a*) and trimer (*b*) encountered in bulk **S** at 298.15 K. Example of an extended H-bonded network and long-range ordering among **S** molecules (*c*). The red dashed lines represent H-bonding interactions and their corresponding distances between hydroxyl groups.

serving as the H-bond donor, as illustrated in Figs. 6*a* and 6*b*.

A detailed analysis reveals that the strength, distribution and lifetime of H-bonds vary significantly between the mixture and its individual components. This variation has a substantial impact on the overall structure and properties of the mixture. Consistent with this observation, the total number of all types of H-bonded complexes — **M-M**, **M-S**, and **S-S** — was found to be 145 only at 298 K. Consequently, the average number of H-bonds per molecule decreased to an unexpectedly low value of 0.29.

These findings suggest that the absence of i ntermolecular interactions, specifically through the supramolecular H-bonding network, can disrupt the crystalline structure of the binary mixture. This change in intermolecular inter-

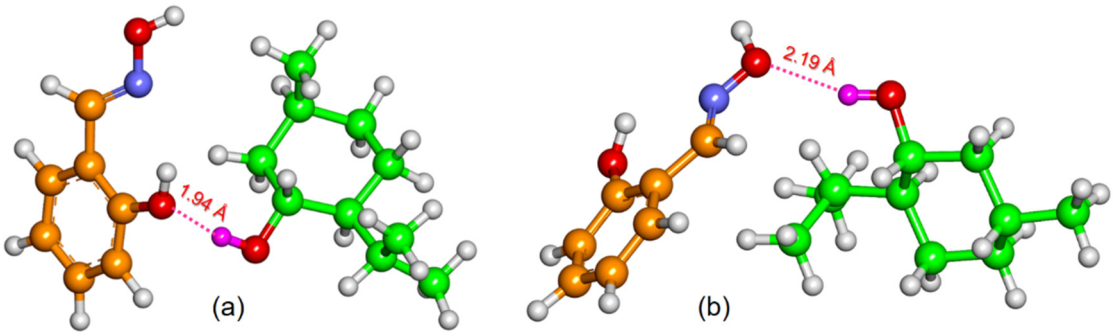

Fig. 6. Representative MD snapshots of H-bonded heterodimers formed by **M** and **S** molecules but with different H-bonding patterns, as observed in their binary mixture at 298.15 K. For more detail, see the legends for Figures 4-5.

actions, from the strong H-bonding present in pure **M** and **S** components to the weaker dispersion and van der Waals interactions prevailing in their binary mixture, may lower the melting point of the mixture. As a result, the mixture can exist as a liquid at room temperature or at moderately elevated temperatures [20].

Radial Distribution Functions. A more detailed analysis of H-bonding interactions was conducted by calculating the pair radial distribution functions (RDF) between specific H-bond donor and acceptor atoms, as summarized in Figures 7a and 7b.

Initially, the RDF profiles were examined for bulk **M** and **S** systems at varying temperatures. The $g(r)$ curve for bulk **M** displays a distinct first peak centered at approximately 0.202 nm, which is attributed to the H_M-O_M pair. The shape and peak position of $g(r)$ are consistent with previously reported studies [40]. Notably, the intensity of this peak decreases with increasing temperature, indicating a partial loss of H-bonding interactions.

Figure 7b presents several $g(r)$ profiles for bulk **S**, indicating H-bonding interactions between the phenol-type hydroxyl group and the aldoxime hydroxylic moiety. The first pronounced peak at 0.184 nm corresponds to the H_A-O_P pair, which is associated with H-bonding between the hydroxyl Hydrogen of the aldoxime (H_A) and the Oxygen atom of the phenyl group (O_P). This $g(r)_{HA\text{-}OP}$ peak confirms the predominance of this type of H-bonding, as illustrated in Figures 5a and 5c. We observed much weaker interactions among the aldoxime hydroxyl groups, evidenced by a low-intensity peak at 0.198 nm in Figure 7*b*. Additionally, other peaks were identified at pair distances greater than 0.25 nm, attributed to the H_P-O_A and H_P-O_P pairs. The low-intensity and shifted peak of $g(r)_{HP\text{-}OP}$ suggests a nearly complete lack of H-bonding interactions between the phenol-type hydroxyl groups. The peak intensities were also decreased with increasing temperature, indicating some breakage of the H-bonding network.

In the binary **M**:**S** mixture, a more complex pair-interaction architecture exists, leading to the consideration of only selected key interaction pairs, as shown in Figure 7c. The strong peak for the H_M-O_P interaction at 0.202 nm supports the earlier analysis, indicating H-bonding between **M** Hydrogen atom (H_M) and the phenolic Oxygen atom (O_A) of *S*, as illustrated in Figures 6*a* and 7*b-c*. Additionally, a second prominent peak for the H_M-O_A pair was observed at 0.231 nm, which is also attributed to H-bonding between **M** Hydrogen atom (H_M) and the aldoxime Oxygen (O_A), as depicted in Figures 6*b* and 7*b-c*. All other $g(r)$ peaks are found beyond the cut-off distance of 0.25 nm, indicating they represent much weaker, long-range non-H-bonding interactions. Most of these peaks decrease in intensity with rising temperature.

4. Summary and Perspectives

The design of deep eutectic mixtures is based on forming a H-bonded network between a H-bond donor and an acceptor [2, 5]. By carefully selecting components, optimizing their proportions, and tailoring interactions, these mixtures can be engineered with specific properties suitable for a wide range of applications. [5-6]. This mechanism makes DESs versatile, sustainable, and highly tunable [19].

In this study, we examined the microstructure and dynamic behavior of the menthol:salicylaldoxime (M:S) mixture using all-atom MD simulations. This system was the focus of our recent experimental study, so here we concen-

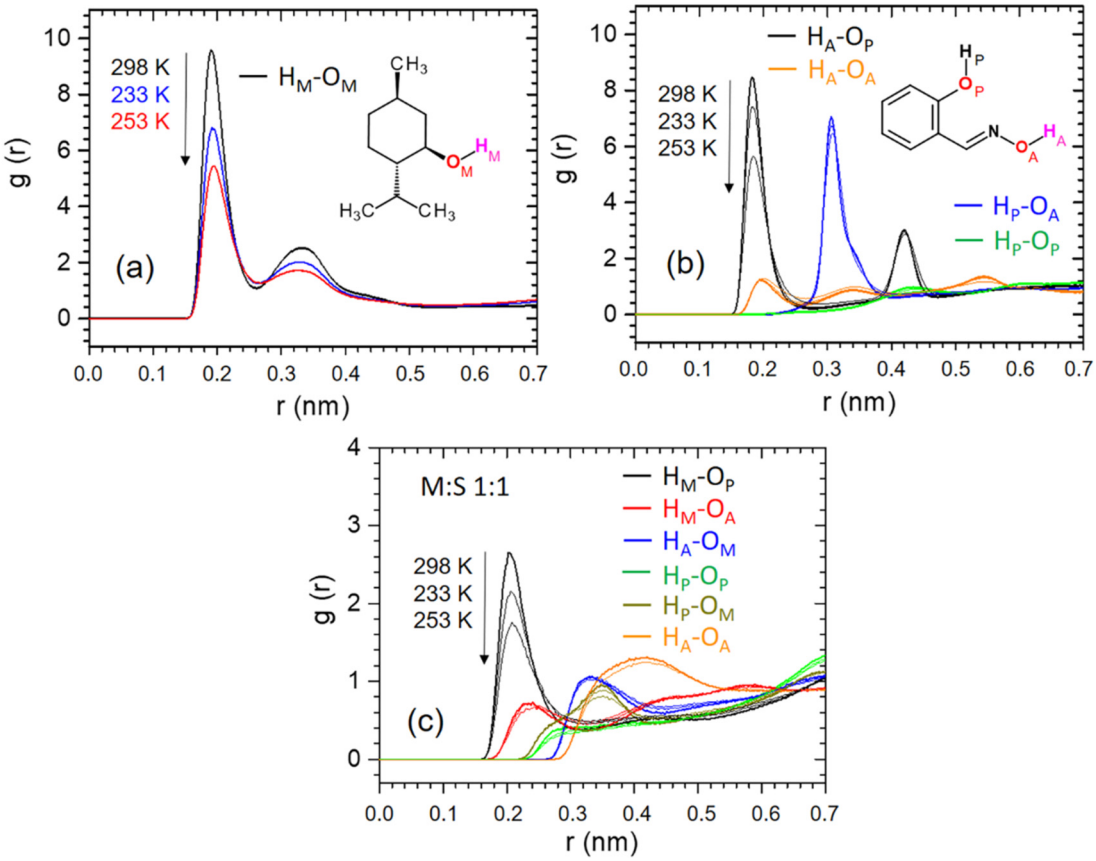

Fig. 7. Radial distribution functions were calculated for atomic pairs in bulk **M** (*a*), **S** (*b*), and their 1:1 mixture (*c*) at various temperatures. The insets in panels *a* and *b* display the structures of the **M** and **S** molecules, highlighting the nomenclature used for the studied atoms.

trated on the temperature-dependent characteristics of the M:S system within the range of 298-353 K at the microscopic level.

We found a nearly uniform distribution of components in the binary M:S mixture at a macroscopic scale, with no phase separation or domain formation detected within the examined temperature range. However, some local microheterogeneity was observed in bulk solid *L*-menthol, characterized by the formation of stable H-bonded complexes ranging from dimers to tetramers. Additionally, solid salicylaldoxime displayed even more extensive H-bonding, where dimers and trimers were relatively minor in comparison. Most interactions contributed to forming an extended, long-range H-bonded network with a three-dimensional architecture. In contrast, in the binary M:S mixture, the formation of H-bond interactions between the components was significantly inhibited. As a result, the transition to a liquid phase at room temperature for the eutectic composition is primarily driven by apolar-apolar attractions between the hydrophobic portions of the constituents.

The change from strong H-bonding in pure component systems to weaker interactions when mixed can explain the significant increase in self-diffusion coefficients D_s. At the molecular level, larger H-bonded tetramers and higher-order clusters, which have complex shapes, typically exhibit lower diffusion coefficients due to increased steric hindrance. When H-bonds break, smaller clusters are formed, allowing for more rapid diffusion and resulting in higher D_s.

Finally, our study highlights that menthol: salicylaldoxime mixtures are characterized by a complex hybrid structural organization of the constituent species, driven by co- and cross-species interactions. We believe that our atomistic MD findings will shed light onto microstructure of menthol-based DES, as a versatile and sustainable alternative to conventional solvents. Continued research and development in this field could unlock new applications and enhance their efficiency and scalability [41, 44].

Acknowledgments: The work was supported with the project of the National Academy of Sciences of Ukraine “New supramolecu-

lar extraction systems for analytical separation, concentration and determination of transition metals". The authors thank all brave defenders of Ukraine who allow us to continue our scientific work.

References

1. M. A. R. Martins, S. P. Pinho, J. A. P. Coutinho. *J. Sol. Chem.* **48** (7), 962-982 (2019).
2. M. Cherniakova, V. Varchenko, K. Belikov. *Chem. Record* **24** (2), e202300267 (2024).
3. T. Khezeli, M. Ghaedi, S. Bahrani *et al.* In *New generation green solvents for separation and preconcentration of organic and inorganic species*, Elsevier, pp 381-423 (2020).
4. P. Makoś, E. Słupek, J. Gębicki. *Microchem. J.* **152**, 104384 (2020).
5. S. E. E. Warrag, M. C. Kroon. In *Deep Eutectic Solvents*, Wiley VCH Verlag GmbH & Co. KGaA., pp 83-93 (2019).
6. M. Zhang, X. Zhang, Y. Liu *et al. Environ. Sci. Pollut. Res.* **28** (27), 35537-35563 (2021).
7. D. O. Abranches, M. A. R. Martins, L. P. Silva *et al. Chem. Commun.* **55** (69), 10253-10256 (2019).
8. M. A. R. Martins, E. A. Crespo, P. V. A. Pontes *et al. ACS Sustainable Chem. Eng.* **6 (7)**, 8836-8846 (2018).
9. A. Abri, N. Babajani, A. M. Zonouz *et al. J. Mol. Liq.* **285**, 477-487 (2019).
10. S. M. Sorouraddin, M. A. Farajzadeh, H. Dastoori. *Talanta* **208**, 120485 (2020).
11. A. Elik, D. Bingöl, N. Altunay. *Food Chem.* **350**, 129237 (2021).
12. D. J. G. P. van Osch, C. H. J. T. Dietz, J. van Spronsen *et al. ACS Sustainable Chem. Eng.* **7** (3), 2933-2942 (2019).
13. W. Tang, K. H. Row. *J. Cleaner Production* **268**, 122306 (2020).
14. T. Ahmadi-Jouibari, N. Noori, N. Fattahi. *Toxin Rev.* **40** (4), 1084-1093 (2021).
15. D. Raj. *J. Chromatogr. A* 1621, 461044 (2020).
16. M. Nedaei, A. R. Zarei, S. A. Ghorbanian. *New J. Chem.* 42 (15), 12520-12529 (2018).
17. M. Y. Cherniakova, O. V. Vashchenko, I. O. Zinchenko *et al. Funct. Mater.* **31** (4), 619–629 (2024).
18. M. Marchel, M. P. Rayaroth, C. Wang *et al. Chem. Engineer. J.* **475**, 144971 (2023).
19. A. Kyriakoudi, I. Radojčić Redovniković, S. Vidović *et al. RSC Sustain.* **2** (6), 1675-1691 (2024).
20. M. Y. Cherniakova, O. V. Vashchenko, J. M. Stolper *et al. New J. Chem.* **48** (33), 14527-14531 (2024).
21. N. Schaeffer, D. O. Abranches, L. P. Silva *et al. ACS Sustainable Chem. Eng.* **9** (5), 2203-2211 (2021).
22. D. K. Panda, B. L. Bhargava. *J. Mol. Graph. Model.* **113**, 108152 (2022).
23. U. L. Abbas, Q. Qiao, M. T. Nguyen *et al. AIChE J.* **68** (1), e17382 (2022).
24. A. Malik, H. K. Kashyap. *J. Chem. Phys.* **155** (4), 044502 (2021).
25. S. Barani pour, J. Jahanbin Sardroodi, A. Rastkar Ebrahimzadeh *et al. Sci. Rep.* **12** (1), 5153 (2022).
26. J. P. Bittner, I. Smirnova, S. Jakobtorweihen. *Molecules* **29** (3), 703 (2024).
27. M. A. Ali, M. A. Kaium, S. N. Uddin *et al. ACS Omega* **8** (41), 38243-38251 (2023).
28. S. Kaur, M. Kumari, H. K. Kashyap. *J. Phys. Chem. B* 124 (47), 10601-10616 (2020).
29. W. L. Jorgensen, J. Tirado-Rives. *Proc Natl Acad Sci USA* **102** (19), 6665-6670 (2005).
30. L. S. Dodda, I. Cabeza de Vaca, J. Tirado-Rives *et al. Nucl. Acids Res.* **45** (W1), W331-W336 (2017).
31. G. Bussi, D. Donadio, M. Parrinello. *J. Chem. Phys.* **126** (1), 014101 (2007).
32. T. Darden, D. York, L. Pedersen. *J. Chem. Phys.* **98** (12), 10089-10092 (1993).
33. B. Hess, H. Bekker, H. J. C. Berendsen *et al. J. Comput. Chem.* 18 (12), 1463-1472 (1997).
34. B. Hess. *J. Chem. Theory Comput.* **4** (1), 116-122 (2008).
35. D. Van Der Spoel, E. Lindahl, B. Hess *et al. J. Comput. Chem.* **26** (16), 1701-1718 (2005).
36. W. Humphrey, A. Dalke, K. Schulten. *J. Mol. Graphics* **14** (1), 33-38 (1996).
37. A. Malik, H. K. Kashyap. *Phys. Chem. Chem. Phys.* **23** (6), 3915-3924 (2021).
38. S. Chatterjee, T. Chowdhury, S. Bagchi. *J. Phys. Chem. B* **128** (51), 12669-12684 (2024).
39. B. D. Ribeiro, C. Florindo, L. C. Iff *et al. ACS Sustainable Chem. Eng.* **3** (10), 2469-2477 (2015).
40. G. Mannucci, M. Busato, A. Tofoni *et al. J. Mol. Liq.* **375**, 121302 (2023).
41. L. de Villiers Engelbrecht, N. Cibotariu, X. Ji *et al. J. Chem. Engineer. Data* **70** (1), 19-43 (2025).
42. A. Kyrychenko, J. Herbich, M. Izydorzak *et al. J. Am. Chem. Soc.* **121** (48), 11179-11188 (1999).
43. A. Kyrychenko, Y. Stepanenko, J. Waluk. *J. Phys. Chem. A* **104** (42), 9542-9555 (2000).
44. P. Makoś-Chełstowska, E. Słupek, S. Fourmentin *et al. Environ. Chem. Lett.* **23** (1), 41-65 (2025).